Numerical Simulation of the Decay of Grid-generated Turbulence in a Shock tube

Mohammad Ali Jinnah

Abstract—**The decay of the grid-generated turbulence has been investigated numerically by solving the time-dependent three-dimensional Navier-Stokes equations with *k-ε* turbulence model for a compressible fluid. Turbulence grids are placed in the shock tube to generate shock induced turbulence in the wake of the grid plate. All turbulent fluctuations are computed along the longitudinal distance in the wake of the grid plate in the shock tube and it is observed that the decay of the turbulence and the decay of Turbulence Kinetic Energy (TKE) level are accelerated along the downstream direction and the percentage of decay depends on the strength of incident shock wave. Due to stronger compressibility effects on decaying turbulent field, all length scales are decreased along the downstream direction. The decay of dissipation rate of TKE is observed along the downstream direction for gradually decreasing the turbulence intensity in the wake of the grid plate.**

Keywords— **Shock wave, Turbulence decay, Navier-Stokes equations, Turbulence model, Turbulent region, Turbulence grids.**

I. INTRODUCTION

In this paper, the investigations on the decay of grid-generated turbulence in the shock tube are conducted and it is one of the innovative works on grid-generated turbulence. Due to turbulence decay, the strength of the turbulence in the wake of the grid plate gradually decreases which may create problems in interaction of reflected shock with homogeneous, isotropic turbulence. After computing the turbulence fluctuations, a numerical simulation was carried out by Jinnah and Takayama (2003) [1] at different strengths of reflected shock wave and it was found that the strength of the turbulence was also changed during interaction with reflected shock wave. The effect of the initial conditions on the decay of homogeneous and isotropic turbulence is still under debate, and there is a substantial body of experimental evidence which would seem to suggest that the initial conditions and the slope of the spectrum, at low wave numbers, determine the value of the decay exponents. It is observed that the actual decay rate of the isotropic turbulence is not only affected by the large scale properties, but also by the small scale properties. An asymptotic similarity state of decaying isotropic turbulence at high Reynolds numbers was predicted by Kolmogorov (1941) [2] based on a supposed dynamical invariant of the flow field

Department of Mechanical and Chemical Engineering, Islamic University of Technology (IUT), BoardBazar, Gazipur-1704, Bangladesh (corresponding author e-mail: jinnah@ iut-dhaka.edu)

found earlier by Loitsianski (1939) [3]. However, it was later shown by Batchelor and Proudman (1956) [4] that the Loitsianski integral is, in fact, not invariant. Furthermore, Saffman (1967) [5] proposed a means of turbulence generation for which this integral diverges. For this Saffman flow, a new invariant was discovered, and a similarity state of decaying homogeneous turbulence at high Reynolds numbers was postulated based on this invariant. Recent large-eddy simulations of decaying isotropic turbulence have confirmed the existence of this exact similarity state to within a few percent. Previous closure calculations and numerical simulations had studied the decay of an initially axisymmetric turbulence in the context of the return-to-isotropy problem by Herring JR. (1974) [6]. The direct numerical simulations performed in the latter two works were necessarily limited to low Reynolds numbers, and the computer resources available at those times allowed only a resolution of 32^3. Previously, Lavoie et al. (2007) [7] investigated potential effects of inflow conditions on the decay of approximately homogeneous isotropic turbulence. Inflow conditions refer to the way the turbulence was generated. In the wind tunnel experiments of these authors, the turbulence was passively generated by square-mesh biplane grids placed at the test section entry. A particular aspect of the potential dependence on inflow conditions was whether the power-law decay of the far downstream turbulence depends on them. Lavoie et al. (2007) [7] tried four different conventional passive grids (with square or with round bars with/without a small helical wire) and two different test sections (one with and one without a secondary contraction to improve isotropy). They did not find any significant effect of inflow conditions on the decay exponent other than that of anisotropy which was, itself, depended on inflow conditions and persisted far downstream. Krogstad and Davidson (2011) [8] carried out a similar wind tunnel study but with two multi-scale grids and one conventional grid. Their grids were all mono-planar and their two multi-scale grids were chosen from one of the three design families of multi-scale grids introduced by Hurst and Vassilicos (2007) [9], specifically the family of fractal cross grids. These grids are very different in design from the low-blockage space-filling fractal square grids which have been used in the vast majority of subsequent works on multi-scale/fractal-generated turbulence and which revealed the possibility of a decaying turbulence without the expected high Reynolds number dissipation scaling.

Many researchers considered the decay of a two-dimensional homogeneous turbulence in a fluid of infinite extent. One of the attractions of studying two-dimensional turbulence was its computational simplicity with respect to

fully developed three-dimensional turbulence. Nevertheless, numerical simulations are still non-trivial, requiring high resolution and long-time integrations, and the asymptotic behavior of the statistics during the decay remains an open problem. Chasnova (1997) [10] contribution was to present some new direct numerical simulation results for decaying two-dimensional turbulence. Particular emphasis was placed on determining the long-time asymptotic evolution of the energy and enstrophy as a function of the initial Reynolds number of the flow field. He considered the asymptotic statistical evolution of the flow field without specifically confronting the existence of coherent vortices or their intermittent distribution in the fluid. This was counter to most current trends in two-dimensional turbulence research. A careful study of the dependence of the decay statistics on the initial Reynolds number of the turbulence may yield some useful information about the physics of the decay. In this previous study, large-eddy simulations were used to confirm theoretical predictions of asymptotic decay laws for the energy and the self-similar decay of the energy spectrum based on low wave number spectral invariants. The higher resolutions obtainable in simulations of two-dimensional turbulence permitted a study of two-dimensional decay at relatively high Reynolds numbers by direct numerical simulations without the need for sub-grid scale modeling. For the present numerical simulation, the three-dimensional Navier-stokes equations using k-ε turbulence model, are solved by shock capturing method where for more accurate solutions, the grid adaptation technique is used. Grid adaptation technique with k-ε turbulence model are the improve technique to determine the turbulence decay in the wake of the turbulence grids.

II. NUMERICAL METHODS

A. Governing Equations

For the present computations, the three-dimensional numerical code is developed to determine the decay of the shock induced turbulence in the shock tube. Without external forces and heat sources, the conservative form of non-dimensionalized governing equation in three-dimensional Cartesian coordinate system is

$$\frac{\partial Q}{\partial t} + \frac{\partial (F-F_v)}{\partial x} + \frac{\partial (G-G_v)}{\partial y} + \frac{\partial (H-H_v)}{\partial z} = S(Q) \quad \dots \quad (1)$$

where $Q = [\rho, \rho u, \rho v, \rho w, e, \rho k, \rho \varepsilon]$, the vector of conservative variables which contains mass, momentum and energy. All variables are calculated in per unit volume. ρ is taken as the mass per unit volume. Three momentum terms in three-dimensional Cartesian coordinates system are ρu, ρv and ρw per unit volume. Total energy, e, turbulent kinetic energy, ρk and turbulent dissipative energy, $\rho \varepsilon$ are the energy terms per unit volume in these computations. F, G and H are the three inviscid flux vectors in x-, y-, and z-axis respectively. Similarly F_v, G_v and H_v are the three viscous flux vectors in x-, y-, and z-axis respectively. Also ρ is the fluid density and u, v and w are velocity components in each direction of Cartesian coordinates. While e is the total energy per unit volume, pressure p can expressed by the following state equation for ideal gas,

$$p=(\gamma-1)[e - \tfrac{1}{2}\rho(u^2+v^2+w^2)] \quad \dots \quad \dots \quad \dots \quad (2)$$

where γ is the ratio of specific heats.
The source term $S(Q)$ of the k-ε turbulence model is written by,

$$S(Q)= [0, 0, 0, 0, 0, P_k - \rho \varepsilon - D_k, (c_{\varepsilon 1} P_k - c_{\varepsilon 2} \rho \varepsilon)\frac{\varepsilon}{k}] \dots \quad (3)$$

where the production term P_k is given in Cartesian coordinates as

$$P_k = \{ 2\mu_t \frac{\partial u}{\partial x} - \frac{2}{3} [\rho k + \mu_t(\frac{\partial u}{\partial x} + \frac{\partial v}{\partial y} + \frac{\partial w}{\partial z})]\} \frac{\partial u}{\partial x} + \{ 2\mu_t \frac{\partial v}{\partial y} - \frac{2}{3}$$

$$[\rho k + \mu_t(\frac{\partial u}{\partial x} + \frac{\partial v}{\partial y} + \frac{\partial w}{\partial z})]\} \frac{\partial v}{\partial y} + \{ 2\mu_t \frac{\partial w}{\partial z} - \frac{2}{3} [\rho k + \mu_t(\frac{\partial u}{\partial x} + \frac{\partial v}{\partial y} +$$

$$\frac{\partial w}{\partial z})]\} \frac{\partial w}{\partial z} + \mu_t(\frac{\partial u}{\partial y} + \frac{\partial v}{\partial x})^2 + \mu_t(\frac{\partial u}{\partial z} + \frac{\partial w}{\partial x})^2 + \mu_t(\frac{\partial w}{\partial y} + \frac{\partial v}{\partial z})^2$$

and the destruction term D_k is given as $D_k = \frac{2\rho}{\gamma.T} k\varepsilon$

The mass average turbulent kinetic energy and homogeneous component of turbulent kinetic energy dissipation rate are defined by as $k = \frac{1}{2} c_t^2 (u^2+v^2+w^2)$ and $\varepsilon = c_m k^2 \frac{Re}{100}$

The various constants in the k-ε turbulence model are listed as follows:
$c_\mu = 0.09$, $c_t = 0.03$, $c_m = 0.09$, $c_{\varepsilon 1} = 1.45$, $c_{\varepsilon 2} = 1.92$, $\sigma_k = 1.00$, $\sigma_\varepsilon = 1.30$

The governing equations described above for compressible viscous flow are discretised by the finite volume method. A second-order, upwind Godunov scheme of Flux vector splitting method is used to discrete the inviscid flux terms and MUSCL-Hancock scheme with k-ε turbulence model is used for interpolation of variables where HLL Reimann solver is used for shock capturing in the flow. Central differencing scheme is used in discretizing the viscous flux terms. The upstream of incident shock wave is set as inflow boundary condition, the properties and velocities of which are calculated from Rankine-Hugoniot conditions with incident shock Mach number. The downstream inflow boundary condition and wall surface are used as solid boundary conditions where the gradients normal to the surface are taken zero. All solid walls are treated as viscous solid wall boundary. For the two-equation k-ε turbulence model on solid boundaries, μ_t is set to zero.

B. Grid System and Grid Adaptation

Three dimensional hexahedral cells with adaptive grids are used for these computations. In this grid system, the cell-edge data structures are arranged in such a way that each cell contains six faces which are sequence in one to six and each face indicates two neighboring cells that is left cell and right cell providing all faces of a cell are vectorized by the position and coordinate in the grid system. The initial three-dimensional grid system with turbulence-generating grids is shown in **Fig.1**. The physical size of each cell before adaptation is equal to 5x5x5 *(mm)* and the initial number of cell is 2876.
The grid adaptation is one of the improved and computational time saving techniques, which is used in these computations.
The grid adaptation is performed by two procedures, one is refinement procedure and another is coarsening procedure. The refinement and coarsening operations are handled separately in computation.
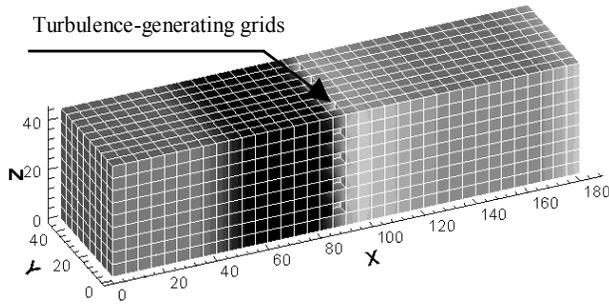
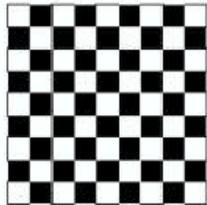Figure 1: Three-dimensional grids and the position of the turbulence-generating grids are shown.

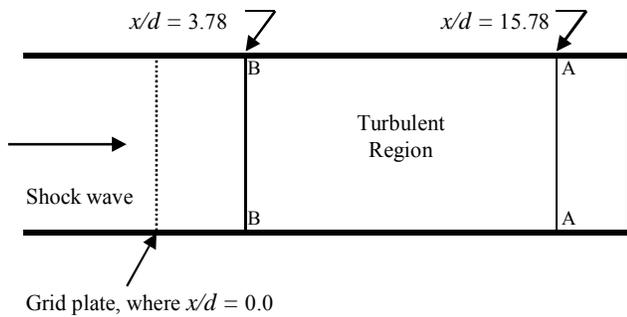Figure 2: The configuration of the turbulence-generating grids in the grid plate.

Figure 3: Sectional view of zx-plane where the location of selected turbulent region is shown.

The criterion used for grid adaptation is based on the truncation error (C_T) of the Taylor series expansion of density. The truncation error indicator C_T is defined for every face of a cell and given by the ratio of the second-order derivative term to the first order one of the Taylor series of density so that

$$C_T = max \left[\frac{|(\nabla \rho)_{lc} - (\nabla \rho)_i|}{(\alpha_f \rho_c)/dl + |(\nabla \rho)_i|}, \frac{|(\nabla \rho)_{lc} - (\nabla \rho)_j|}{(\alpha_f \rho_c)/dl + |(\nabla \rho)_j|} \right]$$

...... (4)

where c represent the location of any face of a cell and i and j represent left cell and right cell of that face, dl is the center distance between cell i and j, $(\nabla \rho)_i$ and $(\nabla \rho)_j$ are the density gradient for cell i and j, $(\nabla \rho)_{lc} = (\rho_i - \rho_j)/dl$, ρ_c is the density at the interface of right cell and left cell and α_f is the constant which is initially designed to prevent a zero denominator. The value of α_f is used 0.02 and it is problem-independent parameter. The refinement and coarsening operation for any cell depends on C_T value and the value of C_T is determined for each face of a cell. The criterion for adaptation for any cell is

Refinement = maximum C_T of six faces of a cell > ε_r
Coarsening = maximum C_T of six faces of a cell < ε_c
where ε_r and ε_c are the threshold values for refinement and coarsening. In these computations, the value of ε_r is used 0.44 and the value of ε_c is used 0.40 and the level of refinement is 2.

In the refinement procedure, the cells are selected for refinement in which every cell is divided into eight new sub cells and these new sub cells are arranged in a particular sequence so that these sub cells are used suitably in the data-structure. In the coarsening procedure, the eight sub cells, which are generated from the primary cell, are restored into the primary cell.

III. RESULTS AND DISCUSSION

For the numerical simulation, turbulence grids are placed in the shock tube parallel to yz-plane and the position of the grid plate is shown in **Fig.1**. The total opening area of grid plate is 50.6 % and the configuration of the grid plate is shown in **Fig.2**. Turbulence grids are uniform in size and spacing, so the shock wave and the gas flow, following the shock wave after passing through turbulence grids, generate a compressible flow of homogeneous, isotropic turbulence and at the same time, the turbulence decay phenomena are happened along the longitudinal direction in the wake of the grid plate.

To compute turbulent parameters in the turbulent region, a selected turbulent region is taken in the wake of the grid plate, which is shown in **Fig.3**. The region between lateral plane AA and BB (parallel to the yz-plane) is taken as the selected turbulent region as shown in **Fig.3** and the centerline along the longitudinal direction (x-axis) of the turbulent region is treated as the centerline of the turbulent region. 30 points of equal spacing are taken on the centerline of the selected turbulent region and all turbulent parameters (velocity fluctuations, pressure fluctuations etc.) are computed on these 30 points for the turbulent region. The lateral planes intersect these 30 points and parallel to the yz-plane are treated as grid-data planes and the grids cut by the grid-data planes (lateral planes on 30 points) are the grids on the grid-data planes. The value of any turbulent parameter on the centerline of the turbulent region is the average value of all the grid values on the grid-data plane where the grids near the boundary are not taken into account due to viscous effect. All the relevant turbulent parameters (velocity fluctuations, pressure fluctuations etc.) are determined along the centerline of the turbulent region for the shock position at the end wall of the shock tube. The longitudinal distances (x/d) of any point on the centerline of the turbulent region are determined from the grid plate where d is the maximum dimensional length of the grids.

The wall pressure fluctuations $<p>/\Delta P$, are calculated from the computed numerical data where the *RMS* value of wall pressure fluctuation,

$$<p> = \sqrt{\frac{\sum_{i=1}^{n} (p_i - P_{av})^2}{n}}$$

where the average pressure, P_{av} is $(1/n)\sum_{i=1}^{n} p_i$, p_i is the instantaneous pressure and n is the number of grids, cut off by the grid-data plane where the grids near the boundary are not taken into account due to viscous effect. ΔP is the pressure difference between upstream and downstream of the shock wave.

Similarly the turbulence intensities, $<u>/\Delta U$ are calculated from the measured numerical data where,
The longitudinal velocity fluctuation in x-axis,

$$u' = \frac{\sum_{i=1}^{n} |u_i - U_{av}|}{n}$$

The *RMS* value of longitudinal velocity fluctuation in x-axis,

$$<u> = \sqrt{\frac{\sum_{i=1}^{n} (u_i - U_{av})^2}{n}} \quad \text{and}$$

Skewness of velocity fluctuation, $S_u = \left(\overline{u^3}\right) / \left(\overline{u^2}\right)^{3/2}$.

The average longitudinal velocity, U_{av} is $(1/n)\sum_{i=1}^{n} u_i$ where u_i is the instantaneous longitudinal velocity. ΔU is the velocity difference between upstream and downstream of the shock wave.
The lateral velocity fluctuation in y-axis,

$$v' = \frac{\sum_{i=1}^{n} |v_i - V_{av}|}{n}$$

The RMS lateral velocity fluctuation in y-axis,

$$<v> = \sqrt{\frac{\sum_{i=1}^{n} (v_i - V_{av})^2}{n}}$$

The average lateral velocity in y-direction, V_{av} is $(1/n)\sum_{i=1}^{n} v_i$ where, v_i is the instantaneous lateral velocity in y-direction. Similarly, the lateral velocity fluctuation in z-axis,

$$w' = \frac{\sum_{i=1}^{n} |w_i - W_{av}|}{n}$$

The RMS lateral velocity fluctuation in z-axis,

$$<w> = \sqrt{\frac{\sum_{i=1}^{n} (w_i - W_{av})^2}{n}}$$

The average lateral velocity in z-direction, W_{av} is $(1/n)\sum_{i=1}^{n} w_i$ where, w_i is the instantaneous lateral velocity in z-direction.

The RMS longitudinal turbulence intensity variations are determined along the centerline of the selected turbulent region in the wake of the turbulence grids. The decay phenomena in 3D turbulent field are observed along the longitudinal direction and the variations of turbulence decay are determined along the longitudinal direction by taking the reference value as an initial value. It is observed in **Fig.4** that the decay rate at the near region of the grid plate is lower and the percentage of longitudinal decay is accelerated as

increasing the longitudinal distance from the grid plate. The approach to isotropy of the flow was assessed by considering the skewness of the velocity fluctuations S_u. From the results of Mohamed and Larue (1990) [11], it is observed that the uncertainty in their measurement of S_u is 0.01, these authors concluded that the position where $S_u = \pm 0.01$ is taken for isotropic flow. According to this recommendation, the present flow appears to be isotropic at all downstream positions where the value of S_u is always less than 0.01 in the turbulent region. The RMS lateral turbulence intensity variations are determined along the centerline of the selected turbulent region in the wake of the turbulence grids. It is observed in **Fig.5-6** that the decay of lateral turbulence intensities along the longitudinal direction are more fluctuating and the lateral turbulence decay phenomena along the longitudinal direction are identical which was explained by Barre et al. (1996) [12] and confirmed that the $<v>$ and $<w>$ components behave in the same way along the lateral direction in the turbulent region.

The decay of pressure fluctuations are determined along the centerline of the selected turbulent region in the wake of the turbulence grids and it is observed that no substantial pressure fluctuations variations occur along the longitudinal direction in the 3D turbulent region.

The dissipative-length scale is defined by the expression, $k^{3/2}/\varepsilon$ where the turbulent kinetic energy, $k = \sum_{i=1}^{n} k_i \Big/ n$ and k_i is the instantaneous turbulent kinetic energy for any grid on the grid-data plane and n is the number of grid on the grid-data plane where the grids adjacent to the boundary are not taken into account due to viscous effect. Similarly the dissipation rate, $\varepsilon = \sum_{i=1}^{n} \varepsilon_i \Big/ n$ where ε_i is the instantaneous TKE dissipation rate for any grid on the grid-data plane. The decay of the dissipative-length scale is determined along the centerline of the turbulent region in the wake of the grid plate which is shown in **Fig.7**. It is observed that no substantial change of the dissipative length scale decay occurs at the near region of the grid plate and the percentage of decay increases gradually as increasing the longitudinal distance. The DNS data of Lee *et al.* (1993) [13] and the DNS data of Hannappel and Friedrich [14] indicated that the velocity length scale and the dissipative length scale increased during expansion process. The DNS results of Lee *et al.* (1994) [15] had indicated a small increase of dissipative length scales through weak shock interactions. Due to stronger compressibility effects, the turbulent dissipative length scale decreases and as decreasing the compressibility effects, the dissipative length scale increases.

The velocity length scale is defined by the expression, $k^{1/2}$. The decay of velocity length scale is determined along the centerline of the turbulent region in the wake of the grid plate which is shown in **Fig.8**. It is observed that no substantial velocity length scale decay occurs at the near region of the grid plate and the decay rate increases gradually as increasing the longitudinal distance.

The decay of the turbulent kinetic energy (TKE) is determined along the centerline of the selected turbulent region which is shown in **Fig.9**. It is observed that the TKE

variations are reasonable for the present turbulent flow with an initial TKE. The TKE evolves towards outlet of the nozzle divergent and it represents the turbulence intensity of the turbulent region. The solution of Navier-Stokes equations provides the information of turbulent kinetic energy (TKE) level in the flow field where the TKE is computed from the equation, $\frac{1}{2}\left(u'^2 + v'^2 + w'^2\right)$ and in this case, the values of TKE are directly related to the velocity fluctuations of the fluid particles. On the other hand, the TKE is obtained from the solution of two equations of k-ε turbulence model and the accuracy of the TKE value depends on the modeling equations. The values of TKE obtained from the velocity fluctuations of the fluid particles in the flow field are compared with the values of TKE obtained from the solution of two equations of k-ε turbulence model because all turbulence modeling equations are not ideal and it must have some deviations between these results.
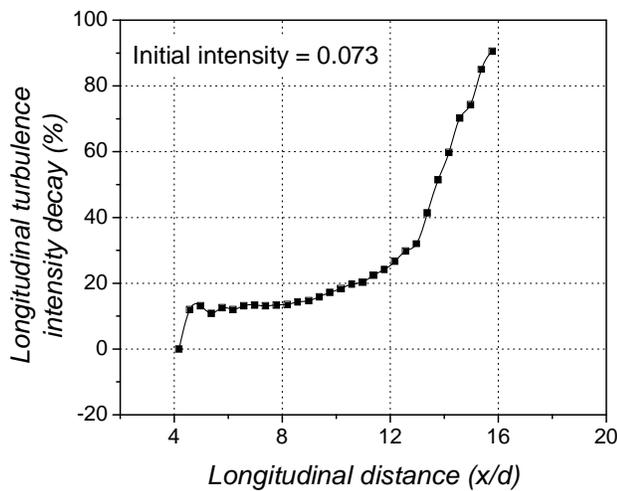
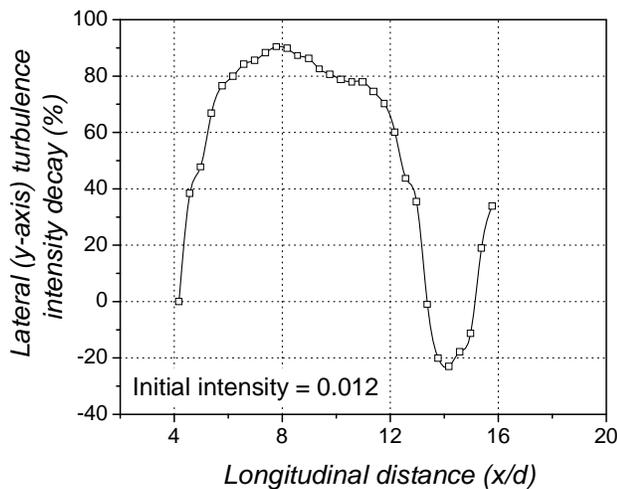Figure 4: The longitudinal turbulence intensity decay along the centerline of turbulent region.

Figure 5: The lateral (y-axis) turbulence intensity decay along the centerline of turbulent region.
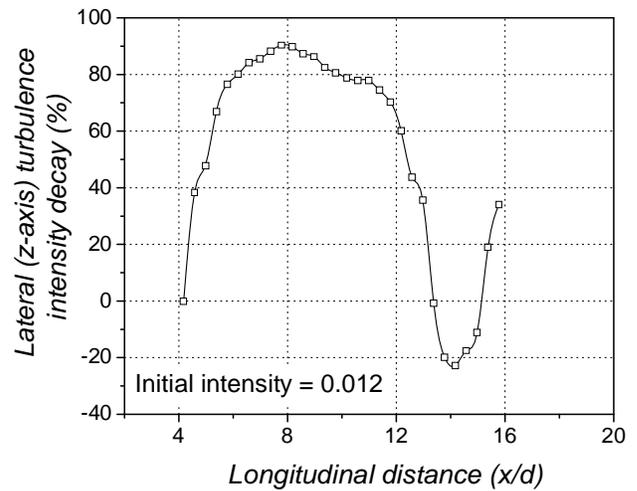
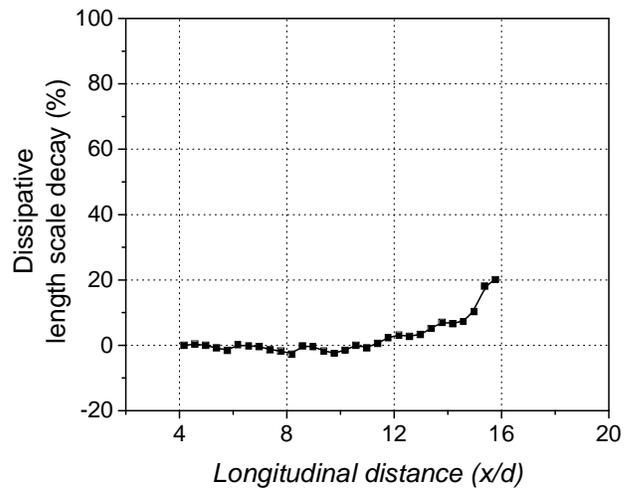Figure 6: The lateral (z-axis) turbulence intensity decay along the centerline of turbulent region.

Figure 7: The decay of dissipative length scale along the centerline of the turbulent region.
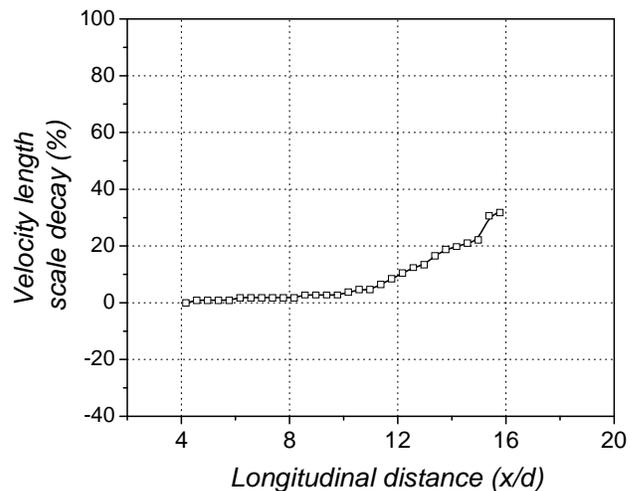
Figure 8: The decay of velocity length scale along the centerline of turbulent region.
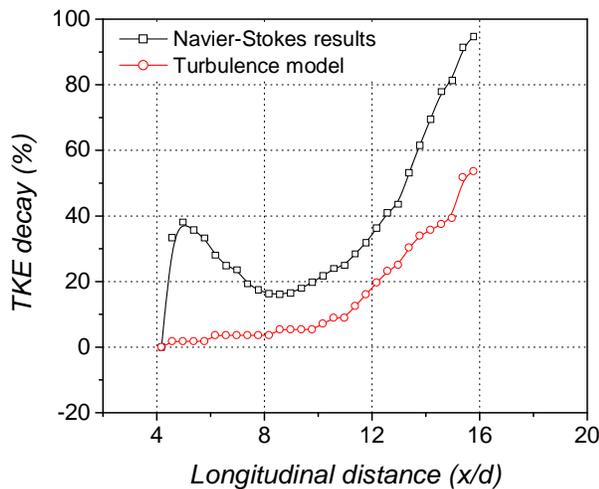
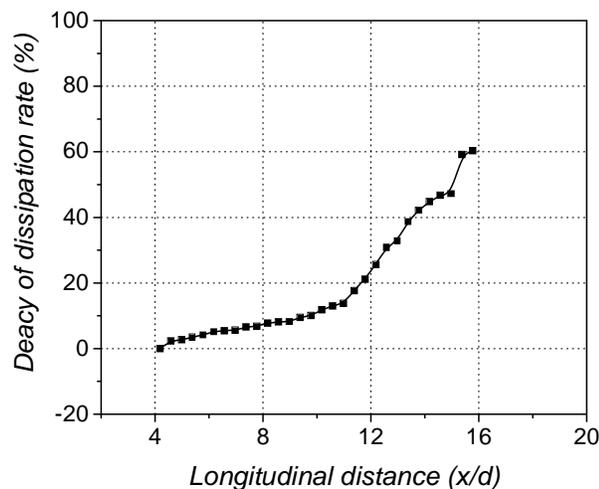Figure 9: The decay of TKE along the centerline of turbulent region.

Figure 10: The decay of dissipation rate of TKE along the centerline of the turbulent region.

The comparisons between the decay of TKE values obtained from the solution of Navier-Stokes equations and the solution of turbulence model are determined along the centerline of the turbulent region and the comparisons are shown in Fig.9 and the deviations between these results are 10-20 %.

The dissipation rate of TKE is changed depending on the compressibility level of the turbulent field and this value vanishes for incompressible flow. Due to shock wave interaction with the turbulent field of stronger compressibility level, the dissipation rate is decreased more and so more dissipation energy converts to thermal energy or internal energy of the flow. The decay of dissipation rate is characterized along the centerline of the turbulent region and the characteristic curve is shown in **Fig.10**. It is observed that the decay of dissipation rate is accelerated as increasing the longitudinal distance. Even though changing of compressibility is very low but due to weaker turbulence fields, the dissipation rate decreases as increasing the longitudinal distance from the turbulence grids.

IV. CONCLUSIONS

A numerical simulation has been conducted to determine the decay of the 3D turbulence in the wake of the turbulence grids along the centerline of the shock tube. The present computational results indicate that the turbulence decaying phenomena in the wake of the turbulence grids are the key factors during interaction with shock, reflected from the end wall of the shock tube. The use of the present technique has the advantage to get the different turbulence fields where the intensity of the turbulence varies along the downstream direction of the shock wave. So due to the turbulence decay, it is possible to get the outcomes of the shock wave interaction with turbulence of different strengths and the interaction results provide the important information on shock wave interaction with different strengths of turbulent fields.

The behavior of turbulence properties are analyzed due to turbulence decay in the wake of the turbulence grids. It is observed from the decaying phenomena that all turbulent length scales decrease and this result agrees with other existing computational results. The dissipation rate of turbulence kinetic energy depends on the turbulence strength and due to turbulence decay along the longitudinal direction; the dissipation rate of TKE is decreased more as increasing the longitudinal distance from the turbulence grids.

REFERENCES

[1] Jinnah MA, Takayama K. (2003) Numerical simulation of shock Mach effect on normal shock/homogeneous turbulence interaction. *Computational Methods and Experimental Measurements XI (Proc. of the eleventh international CMEM-2003 conference)*, pp. 505-515.
[2] Kolmogorov AN. (1941) On degeneration of isotropic turbulence in an incompressible viscous liquid," Dokl. Akad. Nauk. SSSR 31, 538.
[3] Loitsianski LG. (1939) Some basic laws for isotropic turbulent flow. Trudy Tsentr. Aero. Giedrodin. Inst. 440, 31.
[4] Batchelor GK and Proudman I. (1956) The large-scale structure of homogeneous turbulence. Philos. Trans. R. Sot. London 248, 369.
[5] Saffman PG. (1967) The large-scale structure of homogeneous turbulence. J. Fluid Mech. 27, 581.
[6] Herring JR. (1974) Approach of axisymmetric turbulence to isotropy. Phys. Fluids 17, 859.
[7] Lavoie P, Djenidi L and Antonia R. (2007) Effects of initial conditions in decaying turbulence generated by passive grids. J. Fluid Mech. 585, 395–420.
[8] Krogstad PR and Davidson PA. (2011) Freely decaying, homogenous turbulence generated by multi-scale grids. J. Fluid Mech. 680, 417–434.
[9] Hurst DJ and Vassilicos JC. (2007) Scalings and decay of fractal-generated turbulence. Physics of Fluids 19, 035103.
[10] Chasnova JR. (1997) On the decay of two-dimensional homogeneous turbulence, Phys. Fluids **9** (1), pp- 171-80.
[11] Mohamed MS, LaRue JC. (1990) The decay of power law in grid-generated turbulence. *Journal of Fluid Mechanics*; Vol. 219: p-195.
[12] Barre S, Allem D and Bonnet JP. (1996) Experimental study of a normal shock/homogeneous turbulence interaction, AIAA J, 34, pp. 968-74.
[13] Lee S, Lele SK and Moin P. (1993) Direct numerical simulation of isotropic turbulence interacting with a weak shock wave, Journal of Fluid Mechanics, 251, pp. 533-62.
[14] Hannappel R and Friedrich R. (1995) Direct numerical simulation of a Mach 2 shock interacting with isotropic turbulence, Appl. Sci. res., 54, pp. 205-21.
[15] Lee S, Lele SK and Moin P. (1994) Interaction of isotropic turbulence with a strong shock wave. AIAA paper 94-0311, Dept. Mech. Eng., Stanford Univ., CA.